Acta Crystallographica Section D
Biological Crystallography
ISSN 0907-4449

Putative dioxygen-binding sites and recognition of tigecycline and minocycline in the tetracycline-degrading monooxygenase TetX

Gesa Volkers,[a] João M. Damas,[b] Gottfried J. Palm,[a] Santosh Panjikar,[c,d] Cláudio M. Soares[b] and Winfried Hinrichs[a]*

[a]Department of Molecular Structural Biology, Institute for Biochemistry, University of Greifswald, Felix-Hausdorff-Strasse 4, Greifswald, Germany, [b]Instituto de Tecnologia Química e Biológica, Universidade Nova de Lisboa, Avenida da República, 2780-157 Oeiras, Portugal, [c]EMBL Hamburg Outstation, c/o DESY, Notkestrasse 85, Hamburg, Germany, and [d]MX, Australian Synchrotron, 800 Blackburn Road, Clayton, Melbourne, VIC 3168, Australia

Correspondence e-mail: winfried.hinrichs@uni-greifswald.de

Received 21 March 2013
Accepted 19 May 2013

PDB References: TetX, complex with MTC, 4a99; complex with TTC, 4a6n; complex with Xe, 4guv

Expression of the aromatic hydroxylase TetX under aerobic conditions confers bacterial resistance against tetracycline antibiotics. Hydroxylation inactivates and degrades tetracyclines, preventing inhibition of the prokaryotic ribosome. X-ray crystal structure analyses of TetX in complex with the second-generation and third-generation tetracyclines minocycline and tigecycline at 2.18 and 2.30 Å resolution, respectively, explain why both clinically potent antibiotics are suitable substrates. Both tetracyclines bind in a large tunnel-shaped active site in close contact to the cofactor FAD, pre-oriented for regioselective hydroxylation to 11a-hydroxytetracyclines. The characteristic bulky 9-*tert*-butylglycylamido substituent of tigecycline is solvent-exposed and does not interfere with TetX binding. In the TetX–minocycline complex a second binding site for a minocycline dimer is observed close to the active-site entrance. The pocket is formed by the crystal packing arrangement on the surface of two neighbouring TetX monomers. Crystal structure analysis at 2.73 Å resolution of xenon-pressurized TetX identified two adjacent Xe-binding sites. These putative dioxygen-binding cavities are located in the substrate-binding domain next to the active site. Molecular-dynamics simulations were performed in order to characterize dioxygen-diffusion pathways to $FADH_2$ at the active site.

1. Introduction

Tetracyclines (TCs) are used as broad-spectrum antibiotics to treat infectious diseases caused by bacterial pathogens. They bind as an Mg^{2+} complex to the A-site of the bacterial 30S ribosomal subunit and stall ribosomal polypeptide elongation, which results in a bacteriostatic effect (Brodersen *et al.*, 2000; Pioletti *et al.*, 2001). Since the discovery of 7-chlortetracycline (7-ClTC) in *Streptomyces* sp. (Duggar, 1948), several new tetracycline derivatives have been developed. Their intense use and misuse in veterinary and human medicine as well as in industrial livestock farming has caused widespread bacterial resistance mechanisms against tetracyclines (Thaker *et al.*, 2010). Tetracyclines (Fig. 1) have a high variability of substituents at C5–C9 (the hydrophobic edge), whereas substituents at C10–C12 and the A-ring substitution pattern (C1–C4 and C12a; the hydrophilic edge) are conserved to maintain antibiotic activity. Starting from first-generation TCs, the semi-synthetic second generation, which includes minocycline (MTC; Fig. 1) and doxycycline, was developed, with better activity and less susceptibility to resistance. Further modifications to circumvent efflux-based resistance mechanisms resulted in 9-glycylcyclines (Chopra, 2002). Tigecyline (TTC; Fig. 1) has a 9-*tert*-butylglycylamido moiety and represents the most prominent third-generation tetracycline. For a review of tetracyclines, see Nelson & Levy (2011).

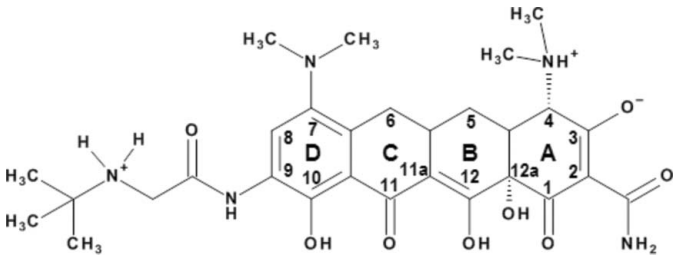

Figure 1
Structure of tigecycline and nomenclature of the tetracycline framework. Tigecycline is denoted as a glycylcycline because of the 9-*tert*-butylglycylamido moiety; the semisynthetic minocycline precursor has only a hydrogen substituent at C9. The keto–enol motif at C11/C12 is deprotonated at pH > 6 to chelate divalent metal ions (Palm *et al.*, 2008).

TTC is able to inhibit ribosomal protein synthesis with a threefold higher efficacy than MTC and a 20-fold higher efficacy than its precursor tetracycline (Olson *et al.*, 2006). To date, only a few resistance determinants against TTC have been identified, such as the AcrAB/TolC multi-drug pumps (Horiyama *et al.*, 2011; Veleba & Schneiders, 2012). The aromatic hydroxylase TetX from *Bacteroides* sp. converts tetracyclines of all generations to 11a-hydroxytetracyclines (Yang *et al.*, 2004). To perform the hydroxylation reaction, the isoalloxazine of the flavin adenine dinucleotide (FAD) cofactor of TetX must be reduced by NADPH followed by oxygenation with dioxygen. This results in a C4a-hydroperoxyflavin which hydroxylates the substrate (see Supplementary Fig. S1[1]). The first reaction product, 11a-hydroxytetracycline, is unable to chelate divalent cations at the former C11/C12 keto–enolate moiety and undergoes subsequent non-enzymatic degradation to a polymer (Yang *et al.*, 2004). This abolishes the affinity for the ribosome. Aerobic bacteria expressing TetX are therefore resistant to tetracyclines, but currently *tetX* is not distributed amongst pathogenic bacteria. It has been shown that TetX can also hydroxylate TTC, which leads to the loss of its antibiotic activity (Moore *et al.*, 2005).

Structures of TetX with FAD and its complexes with the first-generation tetracycline 7-ClTC (aureomycin) and the synthetic 7-iodtetracycline (7-ITC) are known (Volkers, Palm *et al.*, 2011). TetX belongs to the family of FAD-dependent aromatic hydroxylases named after *p*-hydroxybenzoate hydroxylase (*p*HBH) of *Pseudomonas aeruginosa* (Mattevi, 1998). The structural homology of TetX to the *p*HBH family has recently been outlined (see Volkers, Palm *et al.*, 2011 and associated Supporting Online Material).

In this study, we performed X-ray structure analyses of TetX in complex with MTC and TTC, which are clinically important synthetic TCs. The TetX–TTC complex is the first structure of TTC in complex with a protein. This structure shows the binding of TTC in the active site of TetX and explains why TetX is capable of degrading TCs with bulky substituents at the D ring, a common modification that usually leads to a more potent TC compound.

We carried out molecular-dynamics simulations to characterize dioxygen-diffusion pathways to the active-site $FADH_2$. We pressurized TetX crystals with xenon to study dioxygen-binding sites and dioxygen-diffusion pathways, since dioxygen and xenon bind to hydrophobic pockets in proteins (Montet *et al.*, 1997). Comparison of the xenon complex of TetX with the molecular-dynamics simulations allowed us to characterize putative dioxygen-binding sites and dioxygen-diffusion pathways in TetX.

2. Materials and methods

2.1. Protein expression, purification and crystallization

TetX from *B. thetaiotaomicron* was expressed, purified and crystallized in complex with FAD as described previously (Volkers *et al.*, 2010). Native crystals of TetX were soaked with either MTC or TTC for 24–48 h by adding a tiny crystal of the TC to the crystallization droplet. Xenon derivatization of native TetX crystals was performed in a xenon chamber (Hampton Research) using a pressure of 3.5 MPa for 45 s (Panjikar & Tucker, 2002).

2.2. Data collection and processing

Crystals were treated with cryosolutions consisting of 20–25% glycerol in the reservoir buffer for 30 s and flash-cooled in liquid nitrogen. Diffraction data were collected at 100 K on beamline BL14.2 (BESSY synchrotron-radiation source, Berlin, Germany) equipped with a MAR 225 detector. In the case of the xenon derivative, two complete scans were collected from different edges of one crystal to enhance the anomalous signal. Data were reduced and scaled with *XDS* (Kabsch, 2010) and *TRUNCATE* from the *CCP*4 package (Winn *et al.*, 2011).

2.3. Structure determination and refinement

The structures of all TetX complexes were solved by molecular replacement with the polypeptide (383 amino-acid residues) of the isomorphous structure of substrate-free TetX as the starting model (PDB entry 2xdo; Volkers, Palm *et al.*, 2011) and were further refined using *REFMAC*5 (Murshudov *et al.*, 1997, 2011) and *Coot* (Emsley *et al.*, 2010). TLS refinement and noncrystallographic symmetry restraints were applied (Winn *et al.*, 2001). The free *R*-factor calculations were based on 5% of the data excluded from refinement. MTC and TTC were added to the polypeptide models based on their $2F_{obs} - F_{calc}$ and $F_{obs} - F_{calc}$ difference maps. Xe positions were detected by their anomalous signal at a wavelength of 1.5 Å in the anomalous maps calculated with *FFT* and *CAD* (Winn *et al.*, 2011). During model refinement, their occupancies were refined using the 'using SAD data directly' option of *REFMAC*5. The final models were validated using *MolProbity* (Chen *et al.*, 2010). Molecular graphics were created using the *UCSF Chimera* package (Pettersen *et al.*, 2004) and *PyMOL* (DeLano, 2002).

[1] Supplementary material has been deposited in the IUCr electronic archive (Reference: MN5031). Services for accessing this material are described at the back of the journal.

Table 1
Data-collection and refinement statistics.

Values in parentheses are for the highest resolution shell.

Data set	TetX–MTC	TetX–TTC	TetX–Xe
Data collection			
Beamline	BL14.2, BESSY II	BL14.2, BESSY II	BL14.2, BESSY II
Wavelength (Å)	0.91841	0.91841	1.5
Temperature (K)	100	100	100
Space group	*P*1	*P*1	*P*1
Unit-cell parameters (Å, °)	a = 68.87, b = 80.33, c = 86.63, α = 110.82, β = 90.27, γ = 93.39	a = 68.88, b = 80.79, c = 87.65, α = 110.84, β = 89.98, γ = 93.63	a = 68.71, b = 80.14, c = 87.50, α = 111.04, β = 90.06, γ = 93.29
Resolution (Å)	80.94–2.18 (2.31–2.18)	81.90–2.30 (2.42–2.30)	81.64–2.73 (2.80–2.73)
Unique reflections	86443	75168	85826†
Multiplicity	3.75 (3.60)	3.90 (3.90)	3.43 (1.83)
$R_{\rm meas}$ (%)	10.0 (61.9)	10.0 (72.1)	13.3 (57.2)
$\langle I/\sigma(I)\rangle$	11.86 (2.37)	9.10 (2.00)	11.79 (1.74)
Completeness (%)	95.4 (80.4)	96.0 (95.5)	92.8 (60.2)
Wilson B factor (Å^2)	38.4	45.5	54.7
Refinement			
Resolution (Å)	80.94–2.18	81.90–2.30	47.27–2.73
No. of reflections used	82142	71396	41035
$R_{\rm cryst}/R_{\rm free}$‡ (%)	18.4/23.5	21.8/26.0	18.1/22.1
No. of water molecules	640	217	93
R.m.s. deviations from ideality			
Bond lengths (Å)	0.017	0.015	0.013
Bond angles (°)	1.918	1.759	1.683
Average B factor (Å^2)			
Main chain	40.4	70.6	67.5
Side chain	43.1	74.5	70.9
Water	41.5	63.8	49.2
Ramachandran statistics (%)			
Preferred region	96.1	96.0	95.8
Allowed regions	3.5	3.9	3.7
Outliers	0.4	0.1	0.5
PDB code	4a99	4a6n	4guv

† Processed keeping Friedel mates separate. ‡ $R_{\rm free}$ was calculated using 5% of the reflections, which were excluded from refinement.

2.4. Molecular-dynamics simulations

The system of study was TetX in complex with FAD and 7-ClTC (PDB entry 2y6r; Volkers, Palm *et al.*, 2011). For FAD, the fully reduced state $FADH_2$ was considered. Missing atoms of amino-acid side chains as well as the missing loop of residues 246–248 were built with the program *Modeller* (release 9v3; Sali & Blundell, 1993). The protonation states of the Asp, Glu, Lys and Arg residues of TetX were set as the standard states at pH 7 (acids deprotonated, bases protonated). For the protonation of His residues, visual inspection of the structure was used in order to define one of the three possible protonation states by considering neighbouring hydrogen bonds; when the choice was not unequivocal the neutral form was selected. For the molecular-mechanics description of the system, we used the 54A7 GROMOS force field (Schmid *et al.*, 2011), the SPC water model (Berendsen *et al.*, 1981) and a previously parameterized model for dioxygen (Victor *et al.*, 2009) (for details of 7-ClTC and $FADH_2$, see the Supplementary Material). The *GROMACS* 4.5.4 package (Hess *et al.*, 2008) was used for the molecular-dynamics simulations and the simulations were performed on the NPT ensemble using periodic boundaries at standard conditions (further details are given in the Supplementary Material). The protein, together with $FADH_2$ and 7-ClTC, was solvated in a rhombic dodecahedral box, considering a minimum distance of 9 Å to the box walls, ending up with a total of 15 369 water molecules. 12 sodium ions were added to counteract the total charge of the protein. The final system was subjected to a minimization and initialization protocol as described elsewhere (Damas *et al.*, 2011), after which three different replicate molecular-dynamics simulations were run for 16 ns each. The systems were considered to be equilibrated after 10 ns. From the equilibrated portion of the simulations, we sampled three conformations from each replicate simulation (at 12, 14 and 16 ns) for a total of nine different starting conformations. 66 dioxygen molecules were randomly placed within the solvent for each of the nine conformations, and molecular-dynamics simulations were run for 20 ns each. Conformations were saved each picosecond for analysis.

3. Results

3.1. Quality of the model

A complete diffraction data set for TetX in complex with MTC was collected to a resolution of 2.18 Å. The complex of TetX with TTC diffracted to 2.30 Å resolution. Data were collected from a xenon-derivatized TetX crystal to a resolution of 2.73 Å (statistics of data collection and refinement are given in Table 1). The asymmetric unit of the triclinic cell of these TetX complexes contained four monomers. Superpositions of the monomers within the asymmetric unit of each structure

showed root-mean-square differences (r.m.s.d.s) on C^{α} atoms of less than 0.3 Å. The monomers are related by two independent twofold noncrystallographic axes. A crystal-packing analysis has previously been outlined (Volkers, Palm *et al.*, 2011; Volkers *et al.*, 2010). All TCs in the TetX complexes were refined independently with full occupancy.

3.2. Overall three-dimensional structure of TetX

TetX consists of two domains: an FAD-binding domain, which exhibits a Rossmann fold, and a substrate-binding domain. Superpositions of the substrate-free TetX structure (PDB entry 2xdo) onto the TTC complex (PDB entry 4a6n), onto the MTC complex (PDB entry 4a99) and onto the Xe complex (PDB entry 4guv) revealed r.m.s.d.s on C^{α} atoms of only 0.87, 0.94 and 0.87 Å, respectively. Domain motions owing to substrate binding can be ruled out.

The enzyme was crystallized with the oxidized form of the FAD cofactor, which is already in position to bind the substrate. This is true for each TetX structure crystallized to date, but is in contrast to comparable monooxygenases, in which the oxidized and reduced states of FAD correspond to different positions of the isoalloxazine (Gatti *et al.*, 1994).

3.3. The minocycline complex of TetX

3.3.1. Minocycline in the substrate-binding pocket. The substituents of the A ring of MTC form hydrogen bonds comparable to those observed in previously determined TetX complexes (Figs. 2*a* and 2*b* and Supplementary Fig. S2). The A ring of MTC is hydrogen-bonded to the side chain of Gln192. A water molecule serves as a hydrogen-bonding bridge connecting the dimethylammonium at C4 of MTC to the carbonyl O atom Gln192 $O^{\varepsilon1}$, whereas the C3 enolate is hydrogen-bonded to Gln192 $N^{\varepsilon2}$. The position of the water molecule is stabilized by the hydroxyl group of Ser238. As shown previously in the TetX complexes of 7-ITC and 7-ClTC (PDB entries 2y6q and 2y6r), the noncovalently tightly bound cofactor FAD has a large impact on stabilizing substrate binding. The isoalloxazine forms hydrogen bonds *via* its N5 and O4 atoms to the hydroxyl groups at C12 and C12a of MTC. The carbonyl O atom at C1 of MTC hydrogen-bonds to the side chain of Arg213 (Fig. 2*a*). The conserved hydrophilic part of MTC interacts with water molecules, which form hydrogen bonds to protein side-chain and backbone atoms (Fig. 2*b*). MTC does not have any specific substituents at C5, C6, C8 and C9. At position C7 it carries a dimethylamino group which makes van der Waals contacts with the side chains of Met215, Met375 and Phe382 (3.8–4.0 Å). These hydrophobic parts of MTC (C4a–C7) are shielded from the solvent by Phe224, Phe319 and Pro318. The recognition of MTC in the active site of TetX is specific for the conserved substitution pattern of the A ring and C11–C12. This is consistent with the previously observed antibiotic recognition in several structures of TC complexes with proteins such as Tet repressor or EF-Tu (Hinrichs *et al.*, 1994; Heffron *et al.*, 2006) and the prokaryotic ribosomal 30S subunit (Brodersen *et al.*, 2000; Pioletti *et al.*, 2001). A surface representation of TetX reveals that the whole substrate-binding site is divided into a hydrophobic region and a part that exhibits highly hydrophilic properties (Fig. 2*c*). The hydrophobic region is mainly built by the residues of the substrate-binding domain. The hydrophilic part belongs to the FAD-binding domain and only in part to the substrate-binding domain. MTC, like other tetracyclines, fits with its more hydrophobic substituents at C5–C8 in the hydrophobic part of the active site, whereas the conserved hydrophilic substitution pattern at C1–C4 and C10–C12 binds to the hydrophilic surroundings of the active site. Since the hydrophilic moieties of TC are conserved to maintain

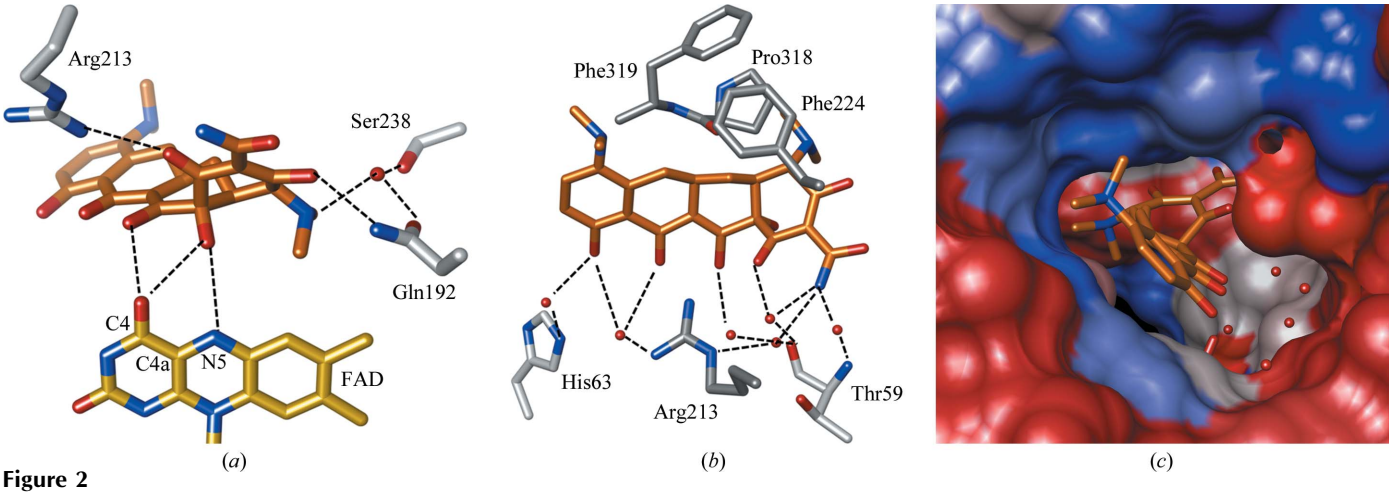

Figure 2
Hydrophilic and hydrophobic recognition of minocycline (MTC) in the active site of TetX. (*a*) Hydrophilic recognition of MTC by the active-site residues of TetX. MTC (orange sticks) shows direct hydrogen-bonding interactions with FAD (yellow sticks) and the side chains of residues Arg213 and Gln192 (with a bridging water molecule; red sphere). Hydrogen bonds in the range 2.6–3.2 Å are indicated by dashed lines. (*b*) Additionally, the conserved hydrophilic part of MTC is hydrogen-bonded *via* water molecules interacting with residues Thr59, His63 and Arg213. MTC is recognized by the hydrophobic residues Phe224, Pro318 and Phe319, which provide a nonpolar environment for the hydrophobic edge of MTC along C5–C7. (*c*) Kyte–Dolittle hydrophobicity surface representation of TetX with hydrophobic residues in blue and hydrophilic residues in red. TetX provides a pocket with its hydrophobic residues of the substrate-binding domain for the hydrophobic edge of MTC along C5–C9 (orange sticks). The hydrophilic edge of MTC located at C1–C4 and C10–C12a interacts with the hydrophilic surroundings of the substrate-binding domain and water molecules.

antibiotic activity, there might be a possibility of developing TC variants with bulky but hydrophilic substituents at C5–C8. Those would interfere with the hydrophobic character and the limited space that is determined by the central β-sheet forming the substrate-binding domain.

3.3.2. Additional minocycline-binding sites. *PISA* analysis of the crystal packing (Krissinel & Henrick, 2007) reveals that the TetX molecules have several different but small interface areas with each other. The surface of the TetX monomer is about 17 200 Å^2 and the largest contact area is only 860 Å^2 for monomers *A* with *D* and *B* with *C*. Thus, quaternary structures are not observed, which is in agreement with the presence of TetX monomers in solution (Yang *et al.*, 2004). Surprisingly, there are two unexpected binding sites for four MTCs with well defined electron density. Both binding sites are located in a cleft formed at the interface of two TetX monomers and are fully occupied by two neighbouring MTC molecules (Figs. 3*a* and 3*b*). The pocket-forming pairs of TetX monomers (*A*/*C* and *B*/*D*) share a contact surface area of only 190 Å^2. At the interface of monomers *A* and *C* of TetX two MTC molecules (MTC.*A* and MTC.*C*) are bound (Fig. 3*a*). Similarly, at the interface of monomers *B* and *D* another cavity is formed for molecules MTC.*B* and MTC.*D*. Both binding sites are equivalent with respect to their position on the surface of the monomers and MTC binding. Thus, discussion can be limited to one case. The MTC dimer is not part of the local twofold symmetry of the corresponding TetX dimer, providing an asymmetric contact surface. MTC.*A* and MTC.*C* are placed with an appropriate orientation of their polar A ring to diffuse into the substrate-entry tunnel of monomer *C* at a distance of about 12–14 Å, whereas the alternative entry of TetX monomer *A* is at least 24 Å away (Fig. 3*a*). Both MTCs also share a larger surface area with TetX monomer *C* (∼225 Å^2) than with TetX monomer *A* (∼170 Å^2).

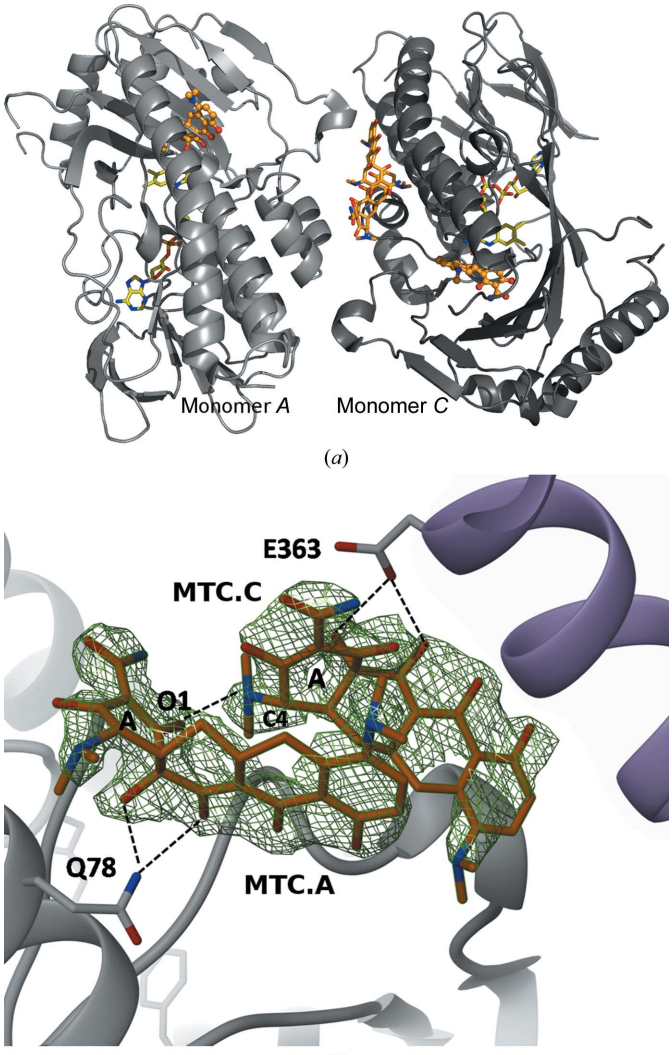

Figure 3
(*a*) Ribbon representation of TetX monomers *A* and *C* with MTCs in the active site represented as ball-and-stick models. Two additional minocycline molecules (MTC.*A* and MTC.*C*) bind at the interface of the TetX monomers in the asymmetric unit. The A rings of both MTCs are much closer to the entrance of the active site of TetX monomer *C* compared with the distance to the entrance of TetX monomer *A*. These MTCs and the FAD cofactor are shown in stick representation. The C atoms of FAD and MTC are coloured yellow and orange, respectively. (*b*) Recognition of MTC in the additional binding site with labelled A rings. MTC.*A* hydrogen-bonds to the side chain of Gln78 and MTC.*C* binds to Glu363. The carbonyl group at C1 of MTC.*A* interacts with the protonated dimethylammonium moiety at C4 of MTC.*C*. The $F_{obs} - F_{calc}$ OMIT map (green) is shown at 3σ. Both MTCs were omitted from the structure-factor calculation. The secondary structures of TetX monomers *A* and *C* are coloured grey and purple, respectively.

The hydrophobic part of both MTCs is covered by a mostly hydrophobic environment provided by both TetX monomers. This is in line with the distinctly hydrophobic properties of MTC compared with other TCs (Griffin *et al.*, 2010). MTC.*A* is covered by side chains Tyr81 and Phe110 of monomer *A* and residues Ser66, Ser326, Val329 and Tyr360 of monomer *C*. MTC.*C* is in contact with the side chains of Ile359 and Tyr350 of TetX monomer *C* and residues Pro106, Glu107 and Phe110 of TetX monomer *A*. The methylene group (C5) of the B ring of MTC.*C* points towards the plane of the π-system of ring D of MTC.*A* (3.4–3.5 Å). Within the MTC dimer, a hydrogen bond from carbonyl O1 (MTC.*A*) to the dimethylammonium at C4 (MTC.*C*) at 2.72 Å compensates the polarity of the A rings to some extent (Fig. 3*b*). Other hydrogen bonds in the range 2.5–3.0 Å are observed from Gln78 N$^{\varepsilon 2}$ of TetX monomer *A* to hydroxyl groups O12 and O12a of MTC.*A*. In MTC.*C* these hydroxyl groups are hydrogen-bonded to Glu363 O$^{\varepsilon 1}$ of TetX monomer *C* (2.57 and 2.75 Å, respectively).

3.4. The tigecycline complex of TetX

The crystal structure of the TetX–TTC complex clarifies that the recognition of TTC by TetX does not differ from that of other tetracyclines (see Supplementary Fig. S2). The electron density reveals that TTC adopts the same orientation in all four TetX monomers, like the other tetracycline derivatives in the active site of TetX (PDB entries 2y6r, 2y6q and 4a99). Comparable to other TetX–TC complexes, the target C11a of TTC is at an appropriate distance of 6.0 Å from C4a at the *re* side of FAD (for nomenclature, see the Supplementary Material and Hanson, 1966). At this distance,

the hydroxylation reaction by the intermediate C4a-hydroperoxyflavin can occur after FAD reduction and dioxygen binding at the *re* side. The 9-*tert*-butylglycylamido moiety leads to a higher susceptibility of the bacterial ribosomal subunit towards TTC combined with an abolished activity of the tetracycline-efflux protein TetA. The 9-*tert*-butylglycylamido substituent of TTC makes no remarkable hydrophobic or hydrophilic contacts with TetX residues. The closest contact for hydrogen bonding of the N atom of the *tert*-butylammonium and the carboxylate of Glu367 is 3.44 Å as observed in TetX monomer *A*, but is up to 5 Å in the other monomers. This rather weak interaction is in agreement with the weak electron density of the flexible 9-*tert*-butylglycylamido substituent, because the 9-*tert*-butylglycylamido group points into the solvent-accessible substrate entrance (Fig. 4). A comparable situation was found for the Mg^{2+} complex of 9-(*N*,*N*-dimethylglycylamido)-6-demethyl-6-deoxytetracycline bound to Tet repressor (Orth *et al.*, 1999). Despite this, TTC shows only common interactions corresponding to the usual binding mode of the A ring to the side chains of Gln192 and Arg213 and the flavin cofactor. The quite hydrophobic part along C5–C8 is bound in a hydrophobic pocket comparable to MTC recognition. This is in line with the observation that the covered surfaces of TTC and all other TCs in the active site of TetX are very similar, ranging from 400 to 430 $Å^2$. Thus, TCs with bulky substituents at position 9 are still susceptible to TetX-mediated resistance. The TetX–TTC complex is another example of the versatile substrate diversity of TetX within the class of tetracycline antibiotics.

3.5. The xenon complex of TetX

A prerequisite for aromatic hydroxylation by flavoproteins is the binding and transfer of dioxygen. After reduction by NADPH, the flavin reacts with dioxygen to produce the hydroxylating intermediate C4a-hydroperoxide (see Supplementary Fig. S1). Therefore, dioxygen must be transferred from the bulk solvent to the inner active site of the monooxygenase. It is well accepted that xenon, a nonpolar species, is able to occupy hydrophobic pockets in proteins under high-pressure conditions (Schiltz *et al.*, 1994) as a result of van der Waals forces. Dioxygen is a hydrophobic species that will also be transferred by binding to hydrophobic pockets in the protein. Such hydrophobic pockets, which are suitable for the binding of dioxygen, can be identified by xenon derivatization of protein crystals. This has recently been demonstrated (Duff *et al.*, 2004; Hiromoto *et al.*, 2006) and was originally intended to be used as a phasing tool for protein structures in macromolecular crystallography (Montet *et al.*, 1997; Wentworth *et al.*, 2001; Svensson-Ek *et al.*, 2002; Panjikar & Tucker, 2002). The refined model of the TetX–Xe complex is highly isomorphous with the model of substrate-free TetX (PDB entry 2xdo), with an r.m.s.d. of 0.9 Å on all polypeptide atoms. In each of the four TetX monomers in the asymmetric unit of the *P*1 cell two Xe positions can be identified by their anomalous signal and strong electron density. Both positions are in the substrate-binding domain, which shields the active site above the isoalloxazine of the FAD cofactor (Fig. 5*a*). There are no xenon-binding sites in the FAD-binding domain. The occupancy for the first binding site (Xe1) ranges from 0.18 to 0.32 within the four monomers; for the second binding site (Xe2) occupancies ranging from 0.51 to 0.71 were found. The distance between Xe1 and Xe2 is about 8 Å. The lower occupied pocket is located near the surface of the protein, whereas the second pocket is closer to the active site. The Xe1 binding site is assumed to be a weaker dioxygen-binding site. The Xe1 binding site is flanked by amino-acid residues that maintain a highly hydrophobic environment (Ile191, Ile237, Phe239, Phe262, Leu263 and Phe267). Similarly, a well defined Xe2 binding site is surrounded by residues Leu223, Phe235, Ile237, Leu263, Phe267, Trp270, Leu277, Tyr274 and Ile278. The pockets share residues Ile237, Leu263 and Phe267.

Both hydrophobic pockets are shielded from the active site by the large β-sheet of the substrate-binding domain consisting of antiparallel strands β12–β15 (Fig. 5*a* and Supplementary Figs. S3 and S4). A search for any direct connection between the Xe positions and the active site using *MOLE* from the *PyMOL* package (DeLano, 2002; Petrek *et al.*, 2006, 2007) did not result in any channels. There are six channels connecting the Xe positions to the solvent and also one that connects the Xe-binding sites (Fig. 5*a*). Any changes in this channel structure upon substrate binding are not obvious because all of the compared crystal structures contained the oxidized form of FAD. Therefore, movement of the side chains seems to be essential for the diffusion of gas molecules from position Xe1 or Xe2 towards the active site.

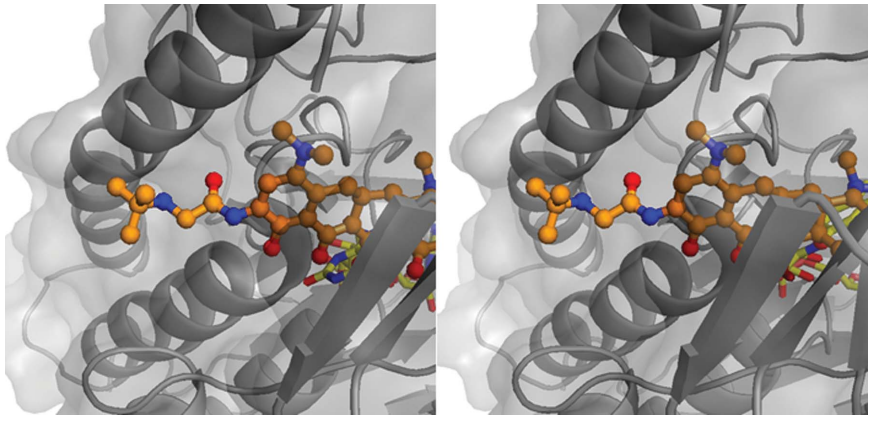

Figure 4
Stereo representation of the TetX complex with tigecycline (ball-and-stick model; hidden FAD in sticks only), which is bound in the active site in the same orientation as other tetracyclines. The view through the β-sheet of the substrate-binding domain shows that the 9-*tert*-butylglycylamido moiety is solvent-exposed and does not interact with protein residues. TetX is shown as a ribbon representation with a transparent surface (grey) for the protein only. The colour code for C atoms is according to Fig. 2.

The binding of dioxygen to other hydrophobic pockets might also be dependent on binding of substrate and NADPH, which changes the hydrogen-bonding potential of the isoalloxazine at N5 upon reduction.

3.6. Molecular-dynamics simulations of dioxygen diffusion

In order to understand how dioxygen reaches the active site from the solvent and the relation to the identified Xe binding sites mentioned above, we modelled the diffusion of dioxygen using standard molecular-dynamics simulations. On initial analysis, when plotting the minimum distance between C4a of FADH$_2$ and dioxygen molecules (which is the reaction pair) along simulation time, it becomes clear that a distance of around 5 Å is reached in almost all replicate simulations (see Supplementary Fig. S5). By the end of the simulation, seven out of nine simulations reached dioxygen distances below 10 Å, with only one replicate simulation never reaching a distance close to 5 Å throughout the entire simulation time. Moreover, the residency time of dioxygen around this 5 Å distance is of many nanoseconds in most simulations. This short distance hints that dioxygen reaches the active site.

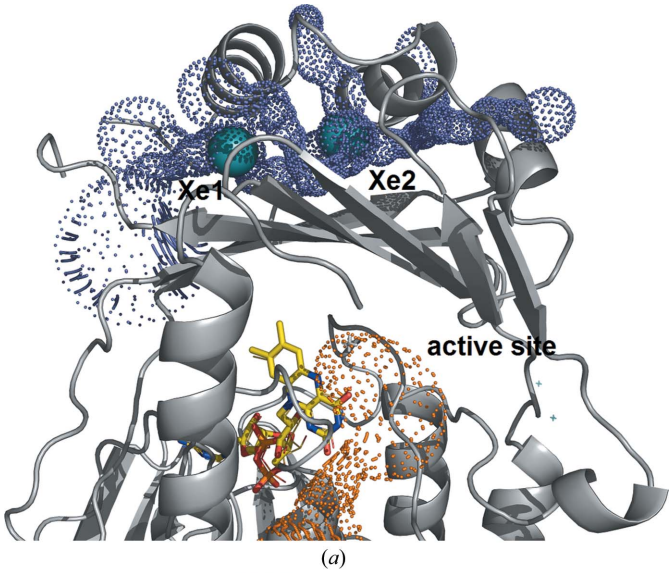

(*a*)

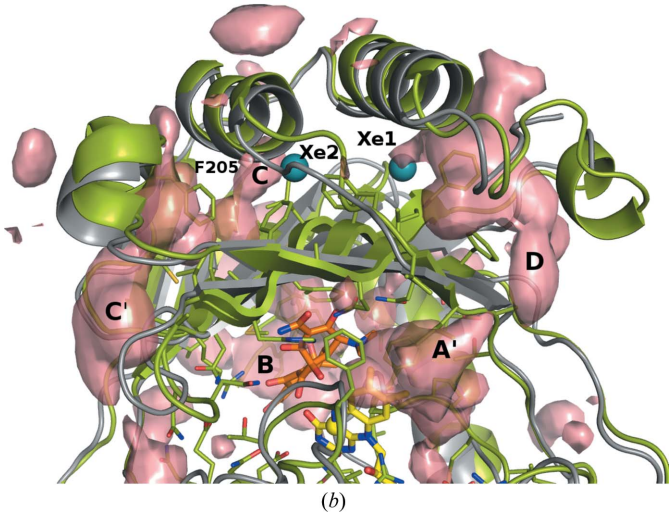

(*b*)

Figure 5
(*a*) Ribbon presentation of the TetX–Xe complex. Xenon-binding sites Xe1 and Xe2 (turquoise spheres) are located in the substrate-binding domain. They are not connected to the active site (orange dots) above the FAD cofactor (yellow sticks). There are channels which connect them to each other and to the outer solvent (blue dots). The channels were detected using *MOLE* from the *PyMOL* package (Petrek *et al.*, 2007; DeLano, 2002). (*b*) Comparison of the dioxygen molecular density isosurface and the xenon-binding sites (turquoise spheres). The viewing direction is opposite to that in (*a*) and is now aligned on C$^{\alpha}$ atoms with the central structure of the molecular-dynamics simulations (green) and dioxygen molecular density (semi-transparent red surface represented as in Fig. 6).

In a more thorough analysis, three-dimensional molecular-density maps were derived from all 594 dioxygen trajectories, allowing the identification of the regions in which it is most probable to find this molecule, *i.e.* the regions with highest affinity for dioxygen. There are two high-affinity regions closest to C4a, A and A′, which are separated by FADH$_2$ and Leu287 (Fig. 6*a*). Region A approaches to about 5 Å from C4a and region B corresponds to the previously described hydrophobic pocket (Volkers, Palm *et al.*, 2011), with 7-ClTc in between this region and C4a. There are also two additional high-affinity regions within the so-called substrate-binding domain: C and D. When comparing the xenon-complex structure with the high-affinity regions (Fig. 5*b*), there is a good correlation between xenon binding sites Xe2 and Xe1 and regions C and D, respectively. The incompleteness in the correlation between the experimental xenon complex and the simulations may arise from the intrinsic difference between dioxygen and the xenon probe and also from the difference between the crystal and the solution environment simulated here. Furthermore, while region C has a spatial relation to region C′ (separated by Phe205), and further down with region B, region D is close to region A′, connecting the Xe1 binding site to region A in the active site through high-affinity regions. This relation is even clearer if we consider all dioxygen trajectories that approach within 5 Å or less of C4a at any time during the simulation and map them onto the high-affinity regions (Fig. 6*b*). This shows that some of these trajectories populate region D. In fact, most trajectories that meet this distance requirement were found to pass through region A′, reaching region A *via* the constriction at Leu287 and FADH$_2$ (Fig. 6*b*). No trajectory shows diffusion of dioxygen from regions B and B′ to the high-affinity region A, probably owing to the presence of the bulky side chain Phe319. This also means that 7-ClTc effectively blocks the possible access of dioxygen to C4a through region B, restricting its access through the other side of the protein (region A′). Therefore, it seems likely that regions A, A′ and D (Fig. 6*b*) are those through which dioxygen passes to enter into the protein and reach C4a of FADH$_2$, with region A on the *re* side of FADH$_2$ being the binding pocket that would favour a face-on reaction with FADH$_2$ (Chaiyen *et al.*, 2012).

4. Discussion

The TetX–MTC and TetX–TTC crystal structures demonstrate specific TetX recognition of a multitude of tetracycline antibiotics. The overall recognition pattern of TCs in the

substrate-binding pocket is very similar on comparing the four available TetX–TC complexes (Supplementary Fig. S2). As shown in Fig. 2(*c*), the hydrophobic and hydrophilic edge of the TC framework fits accordingly to the polarity of the substrate-binding pocket. The hydrophilic part of TCs is in hydrogen-bonding contact with the side chains of Gln192 and Arg213. Furthermore, polar side chains point towards the hydrophilic edge of the TCs and are assumed to be connected by a number of water molecules. Hydrogen bonds from the hydroxyl groups at C12 and C12a to O4 and N5 of the flavin are observed throughout. The distance of C4a at the *re* side of the isoalloxazine to the hydroxylation target C11a of TC is always in the range 5.5–6 Å. After reduction and dioxygenation of the flavin, C4a will become tetrahedral, forcing the isoalloxazine plane to bend. Therefore, further comment on structural rearrangements upon hydroxylation would be too speculative.

The recognition of TTC by TetX is mediated by protein residues binding to the A ring and by FAD, similar to other TetX–TC complexes. The 9-*tert*-butylglycylamido moiety is solvent-exposed, comparable to the 9-glycylcycline complex of TetR (Orth *et al.*, 1999). Unfortunately, this affects new fully synthetic TCs (Charest, Lerner *et al.*, 2005; Charest, Siegel *et al.*, 2005) with bulky substituents at C9 such as the aminomethylcycline amadacycline (Wang *et al.*, 2009) and other recent developments including the fluorocycline TP-434 (Xiao *et al.*, 2012; Grossman *et al.*, 2012). Variation of the D-ring substituents at C8 and C9 will not lead to any tetracyclines that are not susceptible to TetX-mediated hydroxylation. Since the substitution pattern of the A ring is conserved, the development of new tetracyclines in the case of emerging TetX-mediated resistance of pathogens will be difficult.

Chelation of divalent metal ions by the keto–enol motif at C11/C12 of tetracycline (deprotonated at physiological pH; Palm *et al.*, 2008) are not observed in either of the two TetX binding modes, but in the active site the side chain of Arg213 compensates the presumed negative charge. Here, we have to keep in mind that the protonation pattern of TCs may be ambiguous (Aleksandrov *et al.*, 2007). We suggest that the hydroxyl substituents at C12a and of the C11/C12 keto–enol moiety provide another key motif for tetracycline binding in the way that they promote hydrogen bonding to the flavin in the active site and also hydrogen bonds in the surface pocket preformed by TetX packing. The recognition of polar groups of the A ring (O12a, O1, O3 and N4) and O12 is retained even after degradation to isotetracyclines, as observed in corresponding Tet repressor complexes (Volkers, Petruschka *et al.*, 2011).

The additional binding sites for MTC that were identified may play a role in transferring the substrate to the active site of TetX even if the observed binding is promoted by crystal-packing effects and a high MTC concentration during crystal-soaking experiments. Nevertheless, they show how tetracyclines are able to bind to a variety of protein targets. Binding of tetracyclines to different sites of other biopolymers is known for the small ribosomal subunit, which has up to six tetracycline binding sites with varying occupancies (Pioletti *et al.*, 2001), owing to the use of artificially high concentrations for crystal structure determination. Only the site with the highest occupancy is responsible for the antibiotic activity of tetracyclines on the bacterial ribosome (Aleksandrov & Simonson, 2008). Non-antibiotic properties of tetracyclines, on the other hand, are known to include the

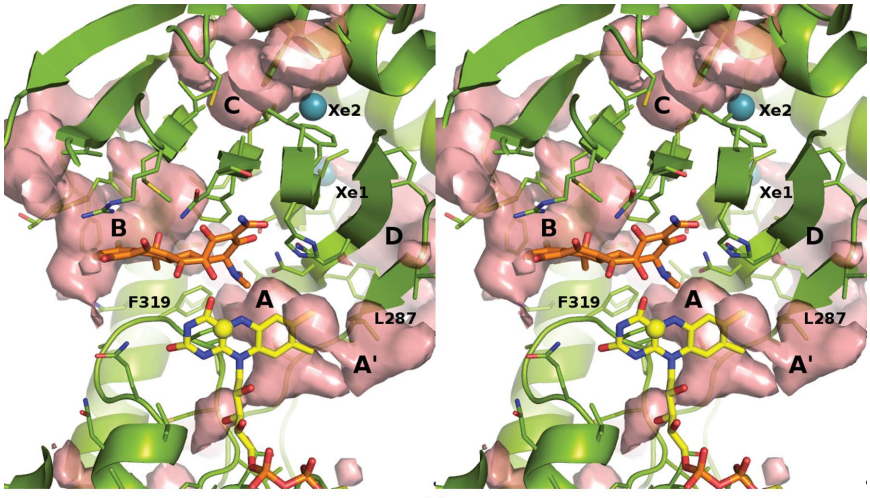

(*a*)

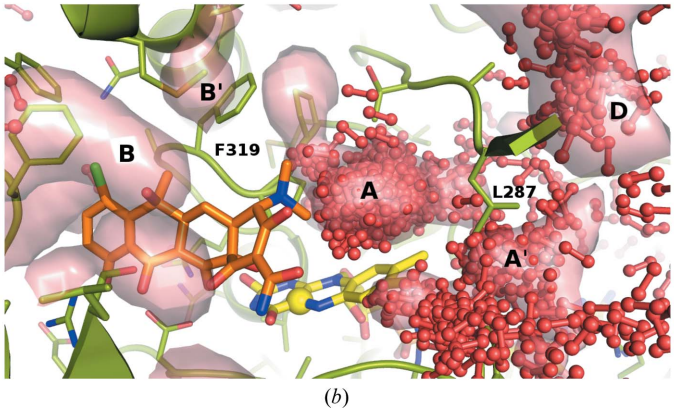

(*b*)

Figure 6
(*a*) Stereoview of dioxygen molecular-density maps and some dioxygen trajectories inside TetX. The TetX model represented here is the conformation that minimizes the r.m.s.d. on Cα atoms. The protein is depicted as a cartoon (green), with $FADH_2$ shown with yellow C atoms and 7-ClTc with orange C atoms, as well as the side chains within a distance of 8 Å around them, which are depicted as sticks. Dioxygen molecular density is represented as a semitransparent red surface enclosing densities of 1×10^{-3} Å^{-3} or higher. C4a of the isoalloxazine is represented as a sphere. (*b*) Additionally, a chosen set of dioxygen trajectories are represented as red spheres and sticks. These trajectories are only those that approach 5 Å or closer to C4a at any time during the simulation. For better visualization, the trajectories represented were sampled every 100 ps.

inhibition of phospholipase A_2, in which MTC is found at a specific site despite having a weak binding constant (Dalm *et al.*, 2010).

Binding and transfer of dioxygen is essential for the activity of monooxygenases. We demonstrate that putative dioxygen-binding sites are located in the substrate-binding domain but are not directly connected to the active site. Nonetheless, entry of dioxygen to the active site was observed in molecular-dynamics simulations using a TetX–TC system. In addition to confirming the xenon-binding sites, the simulations also showed additional high-affinity binding regions. Obviously, the diffusion pathway of dioxygen into the enzyme is not random but is targeted on the active site along specific channels, as has previously been shown for other monooxygenases (Baron *et al.*, 2009). Future experiments with Xe bound to a TetX–TC complex may show these other binding sites for dioxygen that are closer to the active site and that are probably only occupied after substrate binding. Substrate binding prior to the reaction of dioxygen with $FADH_2$ is most probably essential to prevent the oxygenase side reaction which would eliminate H_2O_2 from the C4a-hydroperoxyflavin (Chaiyen *et al.*, 2012).

Recently, adaptive mutants of TetX were discovered by an experimental evolutionary approach in resistant *E. coli* strains that showed increased minimal inhibitory concentrations of MTC *in vivo* (Walkiewicz *et al.*, 2012). Amongst others, two TetX variants with modifications in the substrate-binding domain are characterized by threefold to fivefold increased activities (Phe235Tyr and Thr280Ala). Both amino-acid side chains may interfere with dioxygen diffusion because Phe235 is in close proximity to the binding site of Xe2 (5.2 Å) and Thr280 is C-terminal to an α-helix which participates in the binding pocket of Xe2.

The insertion of oxygen into organic compounds is challenging in chemistry and biotechnology. These crystal structure analyses provide a basis for how this can be performed enzymatically for large aromatic substrates. This will support the understanding and further development of the specific hydroxylation of structurally related compounds.

Beam-time allocation at BESSY II, Berlin is gratefully acknowledged. Fundação para a Ciência e a Tecnologia supported JMD and this work, and JMD through grant PEst-OE/EQB/LA0004/2011 and PhD fellowship SFRH/BD/41316/2007, respectively. GV and JMD received FEBS 'Young Scientist Forum' fellowships, which promoted the interdisciplinary collaboration in this work.

References

Aleksandrov, A., Proft, J., Hinrichs, W. & Simonson, T. (2007). *Chembiochem*, **8**, 675–685.
Aleksandrov, A. & Simonson, T. (2008). *Biochemistry*, **47**, 13594–13603.
Baron, R., Riley, C., Chenprakhon, P., Thotsaporn, K., Winter, R. T., Alfieri, A., Forneris, F., van Berkel, W. J., Chaiyen, P., Fraaije, M. W., Mattevi, A. & McCammon, J. A. (2009). *Proc. Natl Acad. Sci. USA*, **106**, 10603–10608.
Bayly, C. I., Cieplak, P., Cornell, W. & Kollman, P. A. (1993). *J. Phys. Chem.* **97**, 10269–10280.
Berendsen, H. J. C., Postma, J. P. M., van Gunsteren, W. F., DiNola, A. & Haak, J. R. (1984). *J. Chem. Phys.* **81**, 3684.
Berendsen, H. J. C., Postma, J. P. M., van Gunsteren, W. F. & Hermans, J. (1981). *Intermolecular Forces*, edited by B. Pullman, pp. 331–342. Dordrecht: D. Reidel.
Brodersen, D. E., Clemons, W. M., Carter, A. P., Morgan-Warren, R. J., Wimberly, B. T. & Ramakrishnan, V. (2000). *Cell*, **103**, 1143–1154.
Chaiyen, P., Fraaije, M. W. & Mattevi, A. (2012). *Trends Biochem. Sci.* **37**, 373–380.
Charest, M. G., Lerner, C. D., Brubaker, J. D., Siegel, D. R. & Myers, A. G. (2005). *Science*, **308**, 395–398.
Charest, M. G., Siegel, D. R. & Myers, A. G. (2005). *J. Am. Chem. Soc.* **127**, 8292–8293.
Chen, V. B., Arendall, W. B., Headd, J. J., Keedy, D. A., Immormino, R. M., Kapral, G. J., Murray, L. W., Richardson, J. S. & Richardson, D. C. (2010). *Acta Cryst.* D**66**, 12–21.
Chopra, I. (2002). *Drug Resist. Updat.* **5**, 119–125.
Dalm, D., Palm, G. J., Aleksandrov, A., Simonson, T. & Hinrichs, W. (2010). *J. Mol. Biol.* **398**, 83–96.
Damas, J. M., Oliveira, A. S., Baptista, A. M. & Soares, C. M. (2011). *Protein Sci.* **20**, 1220–1230.
Darden, T., York, D. & Pedersen, L. (1993). *J. Chem. Phys.* **98**, 10089.
DeLano, W. L. (2002). *PyMOL* http://www.pymol.org.
Duff, A. P., Trambaiolo, D. M., Cohen, A. E., Ellis, P. J., Juda, G. A., Shepard, E. M., Langley, D. B., Dooley, D. M., Freeman, H. C. & Guss, J. M. (2004). *J. Mol. Biol.* **344**, 599–607.
Duggar, B. M. (1948). *Ann. N. Y. Acad. Sci.* **51**, 177–181.
Emsley, P., Lohkamp, B., Scott, W. G. & Cowtan, K. (2010). *Acta Cryst.* D**66**, 486–501.
Essmann, U., Perera, L., Berkowitz, M. L., Darden, T., Lee, H. & Pedersen, L. G. (1995). *J. Chem. Phys.* **103**, 8577.
Frisch, M. J. *et al.* (2009). *Gaussian* 09, revision A.01. Gaussian Inc., Wallingford, Connecticut, USA.
Gatti, D. L., Palfey, B. A., Lah, M. S., Entsch, B., Massey, V., Ballou, D. P. & Ludwig, M. L. (1994). *Science*, **266**, 110–114.
Griffin, M. O., Fricovsky, E., Ceballos, G. & Villarreal, F. (2010). *Am. J. Physiol. Cell Physiol.* **299**, C539–C548.
Grossman, T. H., Starosta, A. L., Fyfe, C., O'Brien, W., Rothstein, D. M., Mikolajka, A., Wilson, D. N. & Sutcliffe, J. A. (2012). *Antimicrob. Agents Chemother.* **56**, 2559–2564.
Gunsteren, W. F. van, Billeter, S. R., Eising, A. A., Hünenberger, P. H., Krüger, P., Mark, A. E., Scott, W. R. P. & Tironi, I. G. (1996). *Biomolecular Simulation: The GROMOS96 Manual and User Guide.* Zürich: Vdf Hochschulverlag AG an der ETH Zürich.
Hanson, K. R. (1966). *J. Am. Chem. Soc.* **88**, 2731–2742.
Heffron, S. E., Mui, S., Aorora, A., Abel, K., Bergmann, E. & Jurnak, F. (2006). *Acta Cryst.* D**62**, 1392–1400.
Hess, B. (2008). *J. Chem. Theory Comput.* **4**, 116–122.
Hess, B., Kutzner, C., van der Spoel, D. & Lindahl, E. (2008). *J. Chem. Theory Comput.* **4**, 435–447.
Hinrichs, W., Kisker, C., Düvel, M., Müller, A., Tovar, K., Hillen, W. & Saenger, W. (1994). *Science*, **264**, 418–420.
Hiromoto, T., Fujiwara, S., Hosokawa, K. & Yamaguchi, H. (2006). *J. Mol. Biol.* **364**, 878–896.
Horiyama, T., Nikaido, E., Yamaguchi, A. & Nishino, K. (2011). *J. Antimicrob. Chemother.* **66**, 105–110.
Kabsch, W. (2010). *Acta Cryst.* D**66**, 125–132.
Krissinel, E. & Henrick, K. (2007). *J. Mol. Biol.* **372**, 774–797.
Malde, A. K., Zuo, L., Breeze, M., Stroet, M., Poger, D., Nair, P. C., Oostenbrink, C. & Mark, A. E. (2011). *J. Chem. Theory Comput.* **7**, 4026–4037.
Mattevi, A. (1998). *Biophys. Chem.* **70**, 217–222.
Miyamoto, S. & Kollman, P. A. (1992). *J. Comput. Chem.* **13**, 952–962.
Montet, Y., Amara, P., Volbeda, A., Vernede, X., Hatchikian, E. C., Field, M. J., Frey, M. & Fontecilla-Camps, J. C. (1997). *Nature Struct. Biol.* **4**, 523–526.

Moore, I. F., Hughes, D. W. & Wright, G. D. (2005). *Biochemistry*, **44**, 11829–11835.
Murshudov, G. N., Skubák, P., Lebedev, A. A., Pannu, N. S., Steiner, R. A., Nicholls, R. A., Winn, M. D., Long, F. & Vagin, A. A. (2011). *Acta Cryst.* D**67**, 355–367.
Murshudov, G. N., Vagin, A. A. & Dodson, E. J. (1997). *Acta Cryst.* D**53**, 240–255.
Nelson, M. L. & Levy, S. B. (2011). *Ann. N. Y. Acad. Sci.* **1241**, 17–32.
Olson, M. W., Ruzin, A., Feyfant, E., Rush, T. S. III, O'Connell, J. & Bradford, P. A. (2006). *Antimicrob. Agents Chemother.* **50**, 2156–2166.
Orth, P., Schnappinger, D., Sum, P. E., Ellestad, G. A., Hillen, W., Saenger, W. & Hinrichs, W. (1999). *J. Mol. Biol.* **285**, 455–461.
Palm, G. J., Lederer, T., Orth, P., Saenger, W., Takahashi, M., Hillen, W. & Hinrichs, W. (2008). *J. Biol. Inorg. Chem.* **13**, 1097–1110.
Panjikar, S. & Tucker, P. A. (2002). *Acta Cryst.* D**58**, 1413–1420.
Petrek, M., Kosinová, P., Koca, J. & Otyepka, M. (2007). *Structure*, **15**, 1357–1363.
Petrek, M., Otyepka, M., Banás, P., Kosinová, P., Koca, J. & Damborský, J. (2006). *BMC Bioinformatics*, **7**, 316.
Pettersen, E. F., Goddard, T. D., Huang, C. C., Couch, G. S., Greenblatt, D. M., Meng, E. C. & Ferrin, T. E. (2004). *J. Comput. Chem.* **25**, 1605–1612.
Pioletti, M., Schlünzen, F., Harms, J., Zarivach, R., Glühmann, M., Avila, H., Bashan, A., Bartels, H., Auerbach, T., Jacobi, C., Hartsch, T., Yonath, A. & Franceschi, F. (2001). *EMBO J.* **20**, 1829–1839.
Sali, A. & Blundell, T. L. (1993). *J. Mol. Biol.* **234**, 779–815.
Schiltz, M., Prangé, T. & Fourme, R. (1994). *J. Appl. Cryst.* **27**, 950–960.
Schmid, N., Eichenberger, A. P., Choutko, A., Riniker, S., Winger, M., Mark, A. E. & van Gunsteren, W. F. (2011). *Eur. Biophys. J.* **40**, 843–856.
Svensson-Ek, M., Abramson, J., Larsson, G., Törnroth, S., Brzezinski, P. & Iwata, S. (2002). *J. Mol. Biol.* **321**, 329–339.
Thaker, M., Spanogiannopoulos, P. & Wright, G. D. (2010). *Cell. Mol. Life Sci.* **67**, 419–431.
Veleba, M. & Schneiders, T. (2012). *Antimicrob. Agents Chemother.* **56**, 4466–4467.
Victor, B. L., Baptista, A. M. & Soares, C. M. (2009). *J. Biol. Inorg. Chem.* **14**, 853–862.
Volkers, G., Palm, G. J., Weiss, M. S., Wright, G. D. & Hinrichs, W. (2011). *FEBS Lett.* **585**, 1061–1066.
Volkers, G., Petruschka, L. & Hinrichs, W. (2011). *J. Med. Chem.* **54**, 5108–5115.
Volkers, G., Schuldt, L., Palm, G. J., Wright, G. D. & Hinrichs, W. (2010). *Acta Cryst.* F**66**, 611–614.
Walkiewicz, K., Benitez Cardenas, A. S., Sun, C., Bacorn, C., Saxer, G. & Shamoo, Y. (2012). *Proc. Natl Acad. Sci. USA*, **109**, 21408–21413.
Wang, Y., Castañer, R., Bolós, J. & Estivill, C. (2009). *Drug Future*, **34**, 11.
Wentworth, P. Jr, Jones, L. H., Wentworth, A. D., Zhu, X., Larsen, N. A., Wilson, I. A., Xu, X., Goddard, W. A. III, Janda, K. D., Eschenmoser, A. & Lerner, R. A. (2001). *Science*, **293**, 1806–1811.
Winn, M. D. *et al.* (2011). *Acta Cryst.* D**67**, 235–242.
Winn, M. D., Isupov, M. N. & Murshudov, G. N. (2001). *Acta Cryst.* D**57**, 122–133.
Xiao, X.-Y., Hunt, D. K., Zhou, J., Clark, R. B., Dunwoody, N., Fyfe, C., Grossman, T. H., O'Brien, W. J., Plamondon, L., Rönn, M., Sun, C., Zhang, W.-Y. & Sutcliffe, J. A. (2012). *J. Med. Chem.* **55**, 597–605.
Yang, W., Moore, I. F., Koteva, K. P., Bareich, D. C., Hughes, D. W. & Wright, G. D. (2004). *J. Biol. Chem.* **279**, 52346–52352.